mCell V1.0.0 Verilog-A Compact Model

1. Introduction

This model describes the basic switching behavior of a spin-transfer torque (STT) [1]-[3] driven mCell [4]-[8]. The mCell (Fig. 1) is programmed by moving a domain wall (DW) with a current through the write-path of a magnetic nanowire. This magnetization state couples to a free layer in the read-path through an electrically insulating magnetic material, causing the magnetization in each layer to align. The free layer in combination with a tunnel barrier and reference layer forms a magnetic tunnel junction (MTJ) in the read path, setting the resistance of the device. The direction of current through the write-path determines which logic state the device enters. Because the "black-box" model of the mCell is the same regardless of whether the driving force is STT, the spin Hall effect [9]-[12], or something else, this macro-model can be used for any effect so long as the directionality of input current determines the resistance state of an electrically-isolated read-path. However, the parameters (and some empirically-fit behavior) are currently tuned for STT-based domain wall motion.

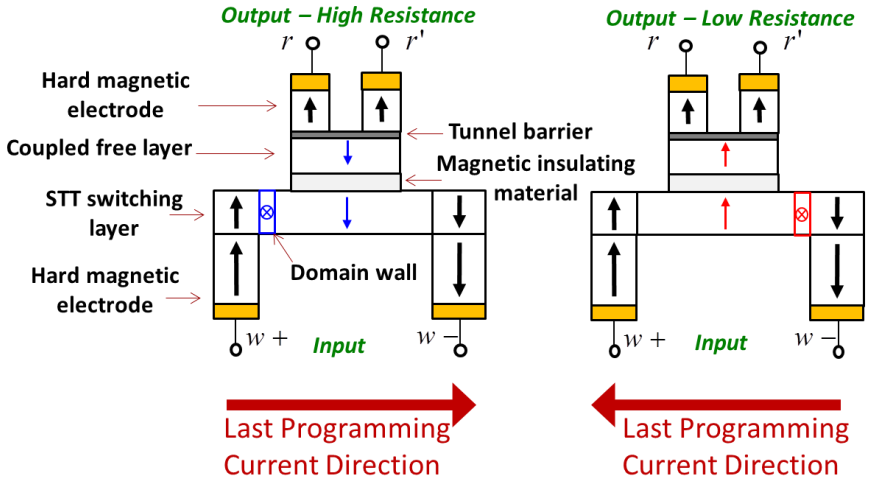

Figure 1 – Cross-section and schematic symbol of mCell. The direction of current through the write-path determines whether the electrically-isolated read-path enters a high or low resistance state.

1.1 Usage Guidelines and Limitations

This model is primarily intended for use in digital transient simulations (i.e., where the pulses are

nominally square in shape). It is not guaranteed to behave correctly for analog applications. Probabilistic switching effects are not modeled. The model will not work for simulations in the frequency domain.

To initiate switching, the current density must exceed a threshold value that is dependent on the pulse width to "depin" the domain wall from its stable end position. We calculate an average value of the write-path current density over a variable time window; if the average value exceeds a calculated depinning time the domain wall is depinned. Micromagnetic simulation was performed to estimate depinning time as a function of current density; the empirical function in the Verilog-A model comes from a fit to the data in Figure 2. This simulation was based on a specific set of device parameters and physical effects; the critical current density and switching time ARE NOT GUARANTEED TO BE CORRECT for all possible mCell parameters (e.g., write-path thickness, interlayer exchange coupling strength, write-path anisotropy, etc.). Additionally, this fit is based on a micromagnetic simulation that modeled pulse widths from 1-10 ns. It is unknown if the trend continues for wider (or shorter) pulses. Lastly, the critical current density and switching time were found to not vary appreciably in a range of width from 10-50 nm (assuming zero edge roughness). It is unknown if these trends continue for wider devices.

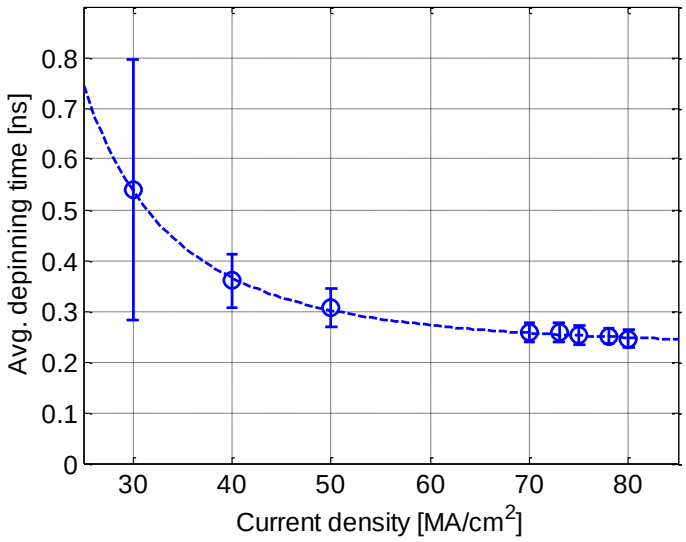

Figure 2 – Micromagnetic simulation of average depinning time as a function of write current density in an STT-mCell.

Once depinning occurs, the velocity of the domain wall is linearly proportional to the current density. This is based on a one-dimensional model of domain wall velocity above Walker breakdown (see Appendix A.1). A flag is available to indicate whether or not the user wishes to simulate the device with two magnetic tunnel junctions (MTJs) in the read-path, or one MTJ and one ohmic contact.

2. Natures and Disciplines

The model defines a "nanokinematic" discipline relating the domain wall position (potential) to its velocity (flow). Units of distance, for input parameters as well as the value of the domain wall position, are given in nanometers. The velocity (flow) units are nanometers/second.

3. Parameters

Very few mCell parameters can be controlled by the user. No material properties or film thicknesses may be varied from device to device. The primary parameters a user is expected to vary are:

- `L_mtj`: the length of a magnetic tunnel junction in the read-path;
- `L_space`: the space between the two MTJs in the read-path;
- `L_ext`: the space between a read-path contact and write-path contact;
- `width`: the width of the device.

A depiction of the length parameters is shown in Figure 3. All units are supplied in nm.

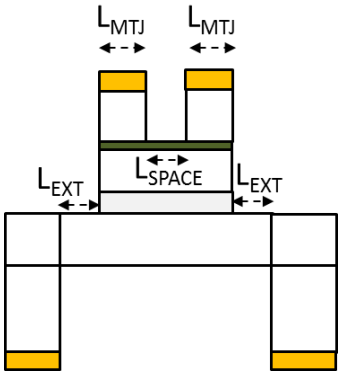

Figure 3 – Definition of length parameters.

The user can also change the value of the MTJ resistance*area (RA) product (`RA_MTJ_low`) and tunnel magnetoresistance (TMR) ratio (`TMR_percent`). The RA is specified in units of $\Omega \cdot nm^2$ and the TMR in %. However, it should be noted that these parameters are not meant to apply to single devices in a design; if these values are adjusted for one device, ALL OTHER DEVICES in the design must use the same values. This is because the RA and TMR are primarily a consequence of film-level properties, particularly the thickness of the tunneling oxide. Although mLogic operation generally tends to benefit from low RA and high TMR, users should input realistic values for these parameters. A TMR exceeding 200% is, to date, unrealistic for room temperature operation, especially at low RA. A good range of values for RA and TMR can be found on papers describing MTJ development for MRAM; see, for example, [13]. The default RA value is already quite low, based off of projections of MTJ properties for 2020 and beyond [14].

Similarly, the user can adjust the value for the resistivity of the write-path (`rho_writepath`), which (along with the geometrical parameters described above) sets the resistance of the write-path. The unit is $\Omega \cdot nm$. Once again, if this value is changed for once device it must be changed for ALL OTHER DEVICES as well. It is recommended that this parameter is left at its default value.

The user also has access to two flag parameters. One of them controls the initial state of the device (`initstate`), such that 0 starts the device in a low resistance state and 1 starts the devices in a high resistance state. The other flag (`ohmic_contact_readpath`) is used to specify how many MTJs appear in the read-path. If the value is 0, two MTJs comprise the read-path; if the value is 1, the read-path contains one MTJ and one ohmic contact. Lower read-path resistance is generally preferable, so having one MTJ to reduce the total resistance may be desirable in most situations. However, ALL DEVICES must have the same `ohmic_contact_readpath` value, because obtaining one ohmic contact in the read-path is likely going to be a global processing step.

Default values for all parameters are specified in the Verilog-A file and reproduced below in Table I. The user should pay careful attention to the units and usage notes.

Table I – Verilog-A parameters and default values.

Parameter	Default Value	Unit	Notes
`L_mtj`	12.0	nm	-
`L_ext`	8.0	nm	-
`L_space`	8.0	nm	-
`width`	10.0	nm	-
`rho_writepath`	200.0	Ω·nm	Must be the same for all devices
`RA_MTJ_low`	1e5	$\Omega \cdot nm^2$	Must be the same for all devices
`TMR_percent`	100.0	%	Must be the same for all devices
`ohmic_contact_readpath`	0	-	Must be the same for all devices; 0 for two MTJs in the read-path, 1 for one MTJ and 1 ohmic contact
`Initstate`	0	-	0 for low resistance, 1 for high resistance

4. Equivalent Circuit Description

The motion of the domain wall in the compact model can be represented by the equivalent circuit in Figure 4. The current source represents the spin-polarized flow of electrons that moves the domain wall. The potential across the capacitor represents the domain wall's position; while the current source is on, the capacitor "charges up" as the domain wall moves across the device. A diode clamping circuit is used to keep the domain wall position bounded between 0 (left end of the write-path) and a maximum position (right end of the device). The absolute value of the maximum position is a function of the lengths described by the user (see section 3), but is represented symbolically as `2*(L_mtj + L_ext) + L_space`. The small shunt conductance is used to model "leakage" of the domain wall position back to 0, but this only occurs when the domain wall is not in a stable end position.

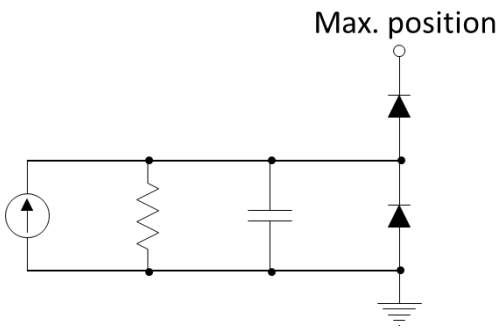

Figure 4 – Equivalent circuit representing domain wall motion.

The resistance of the read-path is a function of the domain wall location. The wall is modeled as having zero width for simplicity. Any MTJ area on the spin-up side of the domain wall is considered to be in the low resistance state and any MTJ area on the spin-down side of the domain wall is considered to be in the high resistance state.

5. Model Equations

This section explains the equations used in the model.

5.1 Domain Wall Velocity

It can be shown (see Appendix A.1) that the velocity of a domain wall driven by spin-transfer torque can be approximated as

$$v_{DW} = \left(\frac{1+\alpha\beta}{1+\alpha^2}\right)\frac{g\mu_B PJ}{2eM_S} = (wall\_speed\_per\_J) * J \quad (1)$$

where α is the Gilbert damping constant, β the nonadiabatic STT coefficient, g the Landé factor, μ_B the Bohr magneton, P the spin polarization, J the electron current density, e the electron charge, and M_s the saturation magnetization. This equation is usually is evaluated in CGS such that the velocity is expressed in cm/sec. In the Verilog-A model, the coefficient `wall_speed_per_J` is calculated at the initial step and converted to units of nm^3/As. This term multiplies the write current density at each time step to set the domain wall velocity in units of nm/s once the wall is depinned.

5.2 Domain Wall Depinning

The idea of the depinning model was introduced in section 1.1. Domain wall depinning is time-dependent, such that large current densities are required to free the wall in a "short" time compared to smaller pulses that are applied for a "longer" time. The actual depinning process is stochastic due to random thermal fluctuations on the magnetization. The depinning time vs. current density profile is also a function of the material properties of the device (including, for example, the perpendicular anisotropy strength of each layer, the thickness of each layer, etc.). Figure 2 is an example profile from simulations of one set of inputs. A "power" fit to the curve was calculated in MATLAB, expressed by the equation:

$$t_{depin} \approx (4523|J|^{-2.82} + 0.2285)\ ns \quad \textbf{(2)}$$

where J is specified in MA/cm^2. Because the current density may be changing over time (if digital pulses are not being used), an average current density is taken in the model. The current density is continually summed from the last zero crossing and divided by the number of time steps from the last zero crossing to get an approximate average value. If the depinning time calculated from equation (2) with the average current density is less than or equal to the amount of time the current has been applied, the domain wall is flagged as depinned. The domain wall is only pinned again when it reaches an end of the device (0 at the left, or the total length at the right). No edge roughness or other defects are modeled that would create pinning sites throughout the write-path.

5.3 Domain Wall Boundaries

Physically, the domain wall is limited in where it can move. The furthest to the left it can be is 0, and the furthest to the right is `2*(L_mtj + L_ext) + L_space`. The "potential" of the capacitor in the equivalent circuit model can be explicitly bounded in these ranges with an `if` statement, but this leads to convergence issues due to the discontinuities that are introduced. For this reason the "diodes" were introduced to the model. They are exponential functions that "turn on" and grow rapidly when the domain wall reaches an end position. These functions were not derived from any model; they are simply introduced to numerically force the domain wall position in a continuous manner.

5.4 Global Minimum "Restoring Force"

With no pinning sites in the write-path, the domain wall has no stable position if it is depinned. The global energy minimum occurs when the domain wall is at its 0 position, because this is where its area is minimized and the magnetostatic energy in the device is also minimized. To capture this effect, another exponential function is used. If the domain wall is not pinned, it experiences a negative drift velocity (maximum speed 0.1 nm/ns) taking the wall back to 0. This effect is also not truly derived from a physical model, but included to approximate this restoring force behavior. It is always present when the domain wall is depinned, but sized so that the current driven component is significantly greater for an appreciable current density.

5.5 Read-Path Resistance

The read-path resistance is set by the domain wall location. For a domain wall position of 0, the resistance is at its minimum value:

$$R_{LOW} = \frac{MTJ\_RA\_low}{width * L\_mtj} \quad (3)$$

When the domain wall is on the opposite end of the device, the resistance is at its maximum value:

$$R_{HIGH} = \frac{MTJ\_RA\_low}{width * L\_mtj}(1 + TMR\_percent) \quad (4)$$

When the domain wall is anywhere between the two read-path electrodes, the resistance is at a midpoint ($(R_{LOW} + R_{HIGH})/2$). When the domain wall is traveling underneath an MTJ electrode, any MTJ area on the spin-up side of the domain wall is considered to be in the low resistance state and any MTJ area on the spin-down side of the domain wall is considered to be in the high resistance state:

```
L_highstate1 = min(L_mtj, max(0, nPos(domain_wall_capacitor)-L_ext));
L_lowstate1 = L_mtj - L_highstate1;
L_highstate2 = min(L_mtj, max(0, nPos(domain_wall_capacitor)-L_ext-L_mtj-L_space));
L_lowstate2 = L_mtj - L_highstate2;
```

6. Transient Simulation

The model was tested in simple SPECTRE benchmark circuits, included online with the model file. The benchmarks are described below. Instructions on how to run the benchmarks can be found in the running_benchmarks.pdf, also included online.

6.1 Single Device Testing

To begin, simple switching tests are used to verify expected mCell behavior. Six cases are included:

(1) A positive current pulse is applied to an mCell in a high resistance state;
(2) A positive current pulse is applied to an mCell in a low resistance state;
(3) A negative current pulse is applied to an mCell in a high resistance state;
(4) A negative current pulse is applied to an mCell in a low resistance state;
(5) A positive current pulse is applied to an mCell in a high resistance state, but its magnitude is too small to fully switch the device in the allotted time;
(6) A positive current pulse is applied to an mCell in a high resistance state, followed by a negative current pulse at a later time.

We expect the following:

(1) Device switches to low resistance state;
(2) Nothing happens (current is not acting to move the domain wall in the opposite direction);
(3) Nothing happens (current is not acting to move the domain wall in the opposite direction);
(4) Device switches to high resistance state;
(5) Device switches to low resistance state, where it remains until the second pulse brings the device back to a high resistance state.

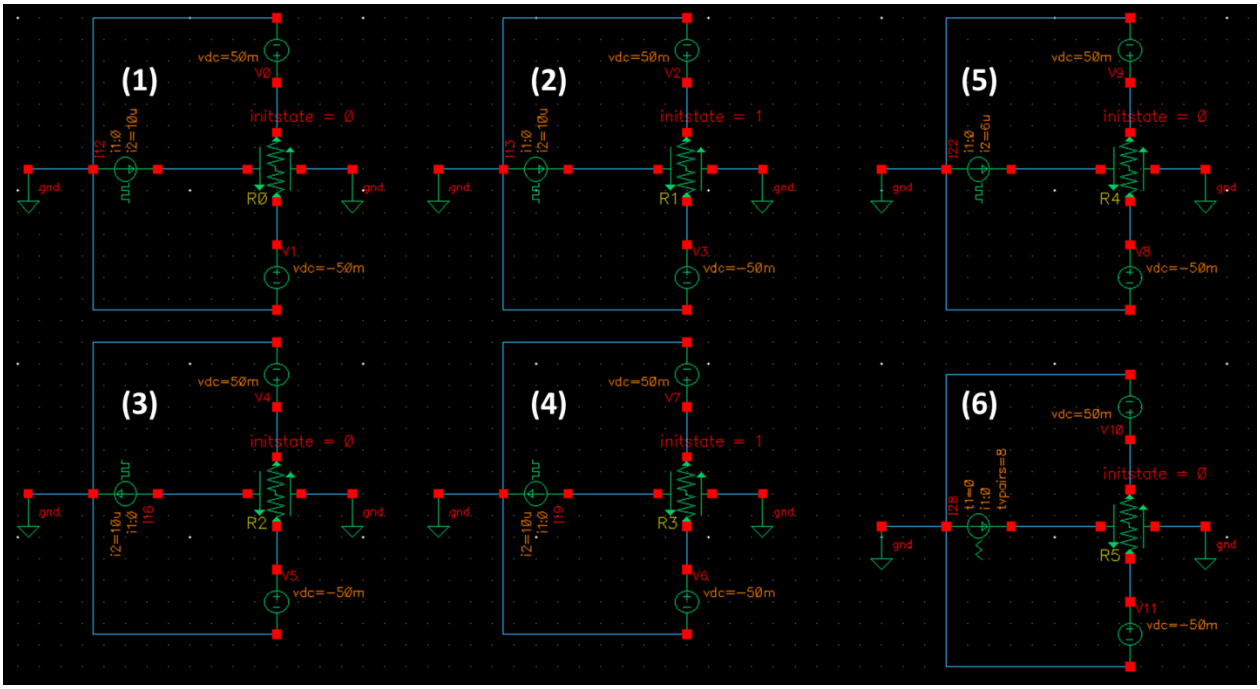

Figure 5 – Schematic of single mCell testbench with different current inputs and initial states.

Waveforms of the read-path resistance as a function of time are shown in Figure 6. The results match expectations.

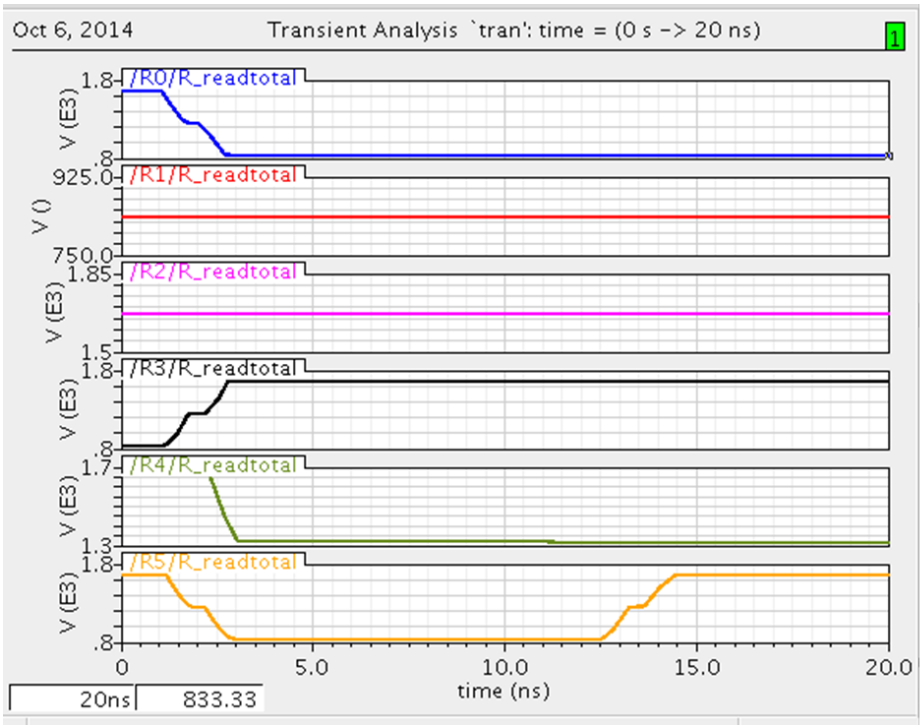

(1) H->L switching

(2) No switching (current in wrong direction)

(3) No switching (current in wrong direction)

(4) L->H switching

(5) Incomplete switching, gradual decay to low R

(6) Back-and-forth digital switching

Figure 6 – Captured waveforms of mCell read-path resistance in each test case. Descriptions labeled on right.

6.2 NAND Gate Driving Inverter

A slightly more complicated test is shown in Figure 7. Here, a two-input NAND gate is connected to drive an inverter. The NAND2 is sized such that the pull-down mCells are three times wider than the pull-up mCells. This is required for the gate to operate correctly for all logical inputs. See [5] for additional details on gate sizing.

We test all four cases of inputs and measure the current flowing into the inverter. In mLogic, the direction of current represents the logical sense of a signal, and so the inputs are current sources directed into or out of the NAND2 inputs. The sign of the output current reflects the logical output of the NAND2 gate. Figure 8 shows the NAND2 output current does indeed follow the expected truth table.

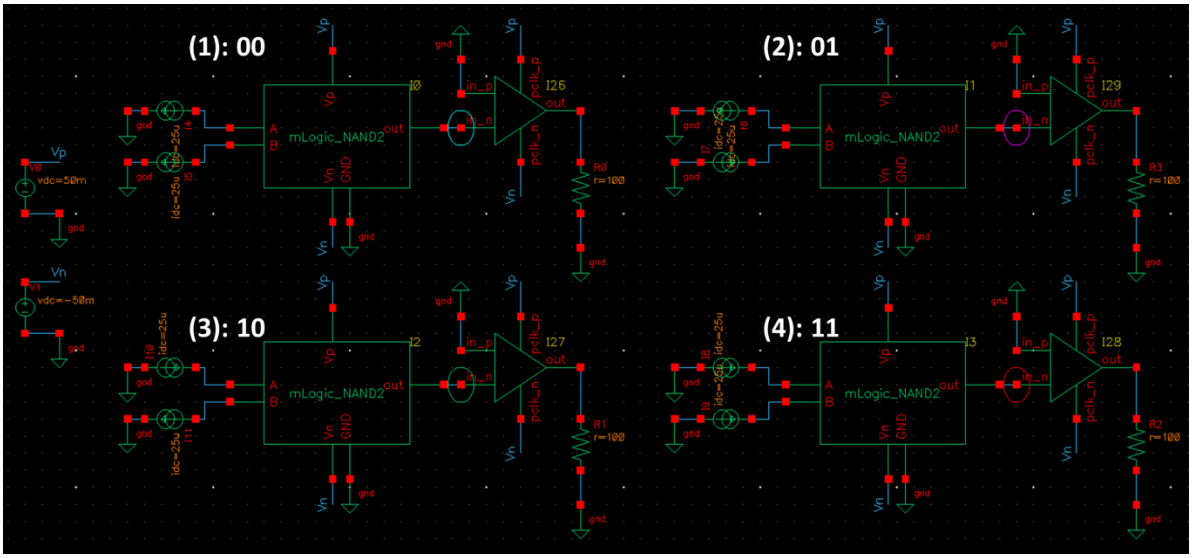

Figure 7 – Schematic of NAND gate driving an inverter for different input cases.

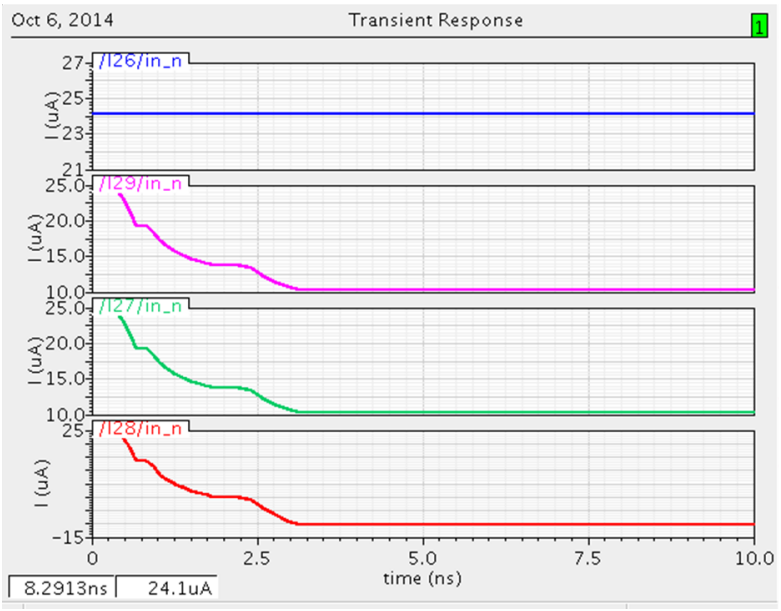

(1) $\overline{0 \cdot 0}$ = 1 (positive output current)

(2) $\overline{0 \cdot 1}$ = 1 (positive output current)

(3) $\overline{1 \cdot 0}$ = 1 (positive output current)

(4) $\overline{1 \cdot 1}$ = 0 (negative output current)

Figure 8 – Captured waveforms of NAND2 test cases. Output current of NAND2 gate is positive when the gate evaluates true and negative when the gate evaluates false.

7. References

[1] L. Berger, "Emission of spin waves by a magnetic multilayer traversed by a current", *Phys. Rev. B,* 54, 9353, 1996.

[2] J. C. Slonczewski, "Current-driven excitation of magnetic multilayers," *Journal of Magnetism and Magnetic Materials*, vol. 159, 1-2, pp. L1-L7.

[3] Z. Li and S. Zhang, "Domain-Wall Dynamics and Spin-Wave Excitations with Spin-Transfer Torques," *Physical Review Letters*, vol. 92, no. 20, pp. 1-4, May 2004.

[4] D. Bromberg, "Current-Driven Magnetic Devices for Non-Volatile Logic and Memory," 2014, Carnegie Mellon University.

[5] D. Morris, "mLogic: Non-volatile Pulsed-Current Logic and Memory Circuits," 2012, Carnegie Mellon University.

[6] D. Morris, D. Bromberg, J.-G. Zhu, L. Pileggi, "mLogic: ultra-low voltage non-volatile logic circuits using STT-MTJ devices," *Proceedings of the 49th Annual Design Automation Conference*, pp. 486-491, 2012.

[7] D. Morris, D. Bromberg, J. Zhu and L. Pileggi, "Magnetic Logic Circuits with Minimal Connections to CMOS," *Proceedings of the IEEE CAS-FEST*, 2012.

[8] D. Bromberg, D. Morris, L. Pileggi, J.-G. Zhu, "Novel STT-MTJ Device Enabling All Metallic Logic Circuits," IEEE Transactions on Magnetics, 2012, 48(11).

[9] J.E. Hirsch, "Spin Hall Effect," *Phys. Rev. Lett*., 83, 1834–1837 (1999).

[10] K.-S. Ryu, L. Thomas, S.-H. Yang, S. Parkin, "Chiral spin torque at magnetic domain walls," *Nature Nanotechnology*, vol. 8, 2013.

[11] S. Emori, U. Bauer, S.-M. Ahn, E. Martinez, G. S. D. Beach, "Current-driven dynamics of chiral ferromagnetic domain walls," *Nature Materials*, vol. 12, 2013.

[12] P. P. J. Haazen, E. Murè, J. H. Franken, R. Lavrijsen, H. J. M. Swagten, B. Koopmans, "Domain wall depinning governed by the spin Hall effect," *Nature Materials*, vol. 12, April 2013.

[13] D. Apalkov, A. Khvalkovskiy, S. Watts, V. Nikitin, X. Tang, D. Lottis, K. Moon, X. Luo, E. Chen, A. Ong, A. Driskill-Smith, M. Krounbi, "Spin-Transfer Torque Magnetic Random Access Memory (STT-MRAM)," *ACM Journal on Emerging Technologies in Computing Systems*, vol. 9, no. 2, article 13, May 2013.

[14] K. C. Chun, H. Zhao, J. D. Harms, T.-H. Kim, J.-P. Wang, C. H. Kim, "A Scaling Roadmap and Performance Evaluation of In-Plane and Perpendicular MTJ Based STT-MRAMs for High-Density Cache Memory," *IEEE Journal of Solid-State Circuits*, vol. 48, no. 2, February 2013.

A.1 1D Model of Domain Wall Velocity

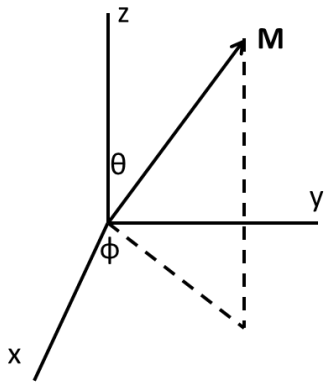

Figure A.1.1 – Illustration of spherical coordinate system used in calculation.

For a one-dimensional current flow in the x-direction, the Landau-Lifshitz-Gilbert equation that governs magnetization dynamics simplifies to:

$$\frac{\partial \vec{M}}{\partial t} = -\gamma \vec{M} \times \vec{H}_{eff} + \frac{\alpha}{M_s}\vec{M} \times \frac{\partial \vec{M}}{\partial t} + \frac{1}{M_S^2}\vec{M} \times \left(\vec{M} \times u\frac{\partial \vec{M}}{\partial x}\right) + \frac{\beta}{M_s}\vec{M} \times u\frac{\partial \vec{M}}{\partial x} - \frac{\gamma}{M_S}\vec{M} \times \left(\vec{M} \times H_{SHE}\hat{y}\right) \quad \textbf{(5)}$$

where $\vec{M}$ is the magnetization vector, M_s the saturation magnetization, $\vec{H}_{EFF}$ the effective magnetic field acting on the magnetization (due to an applied field, anisotropy, exchange, and demagnetization), α the Gilbert damping constant, β the nonadiabatic STT strength, and $u = \frac{g\mu_B PJ}{2eM_s}$, with the same definitions given in section 5.1. We include a spin Hall effect torque term for completeness; $H_{SHE} = \frac{\hbar J_{NM}\theta_{SH}}{2eM_s t_{FM}}$, where $\hbar$ is the reduced Planck constant, J_{NM} the current density in a non-magnetic underlayer, θ_{SH} the spin Hall angle, and t_{FM} the thickness of the ferromagnetic layer in the write-path.

In a spherical coordinate system (Figure A.1.1), we can represent the time rate of change of the magnetization in terms of the polar angle θ and the azimuthal angle φ:

$$\frac{\partial \hat{\theta}}{\partial t} = \dot{\theta} = -\frac{\gamma}{M_s}\vec{\tau}_\theta \quad \textbf{(6a)}$$

$$\frac{\partial \hat{\varphi}}{\partial t} = \dot{\varphi} = -\frac{\gamma}{M_s}\vec{\tau}_{\varphi} \quad \textbf{(6b)}$$

Where $\vec{\tau}_{\theta}$ and $\vec{\tau}_{\varphi}$ are the net torques in the theta and phi directions. These torques represent all terms in Equation (5) – one due to the effective field (applied field, demagnetizing field, anisotropy field, and exchange field), one due to a "damping field," the adiabatic and nonadiabatic spin torques, and the SHE torque.

A.1.1 Torque Calculations

The magnetization vector at the domain wall center can be described in terms of its angle and magnitude as:

$$\vec{M} = M_s(\sin\theta\cos\varphi\ \hat{x} + \sin\theta\sin\varphi\,\hat{y} + \cos\theta\,\hat{z}) \quad \textbf{(7)}$$

Any conversions from Cartesian to spherical coordinates use the following rotation matrix:

$$\begin{bmatrix} a_R \\ a_\theta \\ a_\varphi \end{bmatrix} = \begin{bmatrix} \sin\theta\cos\varphi & \sin\theta\sin\varphi & \cos\theta \\ \cos\theta\cos\varphi & \cos\theta\sin\varphi & -\sin\theta \\ -\sin\varphi & \cos\varphi & 0 \end{bmatrix} \begin{bmatrix} a_x \\ a_y \\ a_z \end{bmatrix} \quad \textbf{(8)}$$

A.1.1.1 Torque Due to Applied Field

Generally speaking, no applied fields are required for mCells to operate. For the sake of completeness, we will include an applied field in this discussion, taking the form:

$$\vec{H}_{APP} = H_x\hat{x} + H_y\hat{y} + H_z\hat{z} \quad \textbf{(9)}$$

By taking a cross product with Equation (7) we obtain:

$$\vec{M} \times \vec{H}_{APP} = \begin{bmatrix} H_z\sin\theta\sin\varphi - H_y\cos\theta \\ -H_z\sin\theta\cos\varphi + H_x\cos\theta \\ H_y\sin\theta\cos\varphi - H_x\sin\theta\sin\varphi \end{bmatrix} = \vec{\tau}_{H_{APP}} \quad \textbf{(10)}$$

Using the rotation matrix of Equation (8) we can express this in spherical coordinates as:

$$\vec{\tau}_{H_{APP}} = \begin{bmatrix} 0 \\ H_x \sin\varphi - H_y \cos\theta \\ H_x \cos\theta \cos\varphi + H_y \cos\theta \sin\varphi - H_z \sin\theta \end{bmatrix} M_S \tag{11}$$

A.1.1.2 Torque Due to Demagnetizing Field

The demagnetizing field inside and around a magnetic structure is generally quite complex. For this analysis, we will approximate the wire in which the domain wall resides as having demagnetizing factors N_x, N_y, N_z in the $\hat{x}$, $\hat{y}$, and $\hat{z}$ directions. With this approximation, the demagnetizing field may be expressed as:

$$\vec{H}_D = -4\pi \overleftrightarrow{N}_D \vec{M} = -4\pi M_s \left(N_x \sin\theta \cos\varphi \, \hat{x} + N_y \sin\theta \sin\varphi \, \hat{y} + N_z \cos\theta \, \hat{z} \right) \tag{12}$$

Taking a cross product with $\vec{M}$ (Equation (7)) and converting to spherical coordinates yields a torque of:

$$\vec{\tau}_{DMG} = \begin{bmatrix} 0 \\ \left(N_y - N_x\right) \sin\theta \sin\varphi \cos\varphi \\ \sin\theta \cos\theta \left(N_z - N_y \sin^2\varphi - N_x \cos^2\varphi \right) \end{bmatrix} 4\pi M_s^2 \tag{13}$$

A.1.1.3 Damping Torque

Magnetization damping at the domain wall center is phenomenologically described by the second term of Equation (5). We can decompose the time derivative of the magnetization as follows:

$$\frac{\partial \vec{M}}{\partial t} = \frac{\partial M}{\partial \theta}\frac{\partial \theta}{\partial t} + \frac{\partial M}{\partial \varphi}\frac{\partial \varphi}{\partial t} = \dot{\theta}\frac{\partial M}{\partial \theta} + \dot{\varphi}\frac{\partial M}{\partial \varphi} \tag{14}$$

The derivatives of the magnetization with respect to angle can be computed from Equation (7) and then plugged in:

$$\frac{\partial M}{\partial \theta}\frac{\partial \theta}{\partial t} = \dot{\theta}\cos\theta\cos\varphi\,\hat{x} + \dot{\theta}\cos\theta\sin\varphi\,\hat{y} - \dot{\theta}\sin\theta\,\hat{z} \quad \textbf{(15a)}$$

$$\frac{\partial M}{\partial \varphi}\frac{\partial \varphi}{\partial t} = -\dot{\varphi}\sin\theta\sin\varphi\,\hat{x} + \dot{\theta}\sin\theta\cos\varphi\,\hat{y} - 0\hat{z} \quad \textbf{(15b)}$$

By computing the torque as $\vec{\tau}_\alpha = -\frac{\alpha}{\gamma M_s}\left(\vec{M} \times \frac{\partial \vec{M}}{\partial t}\right)$ and converting to spherical coordinates, we obtain:

$$\vec{\tau}_\alpha = \begin{bmatrix} 0 \\ \dot{\varphi}\sin\theta \\ -\dot{\theta} \end{bmatrix} \frac{\alpha M_s}{\gamma} \quad \textbf{(16)}$$

A.1.1.4 Torque Due to Anisotropy and Exchange Fields

For perpendicular anisotropy (along the z-axis), the anisotropy field is given by:

$$\vec{H}_k = \frac{2K}{M_s^2}\left(\vec{M}\cdot\hat{a}\right)\hat{a} = \frac{2K}{M_s}\cos\theta\,\hat{z} \quad \textbf{(17)}$$

The torque then can be expressed as:

$$\vec{M} \times \vec{H}_k = 2K(\sin\theta\cos\theta\sin\varphi\,\hat{x} - \sin\theta\cos\theta\cos\varphi\,\hat{y} + 0\hat{z}) \quad \textbf{(18)}$$

The exchange field, which expresses the exchange energy acting to align neighboring magnetic moments in terms of a magnetic field, can be expressed as:

$$\begin{aligned} \vec{H}_{ex} = \frac{2A}{M_s^2}\vec{\nabla}^2\vec{M} &= \frac{2A}{M_s^2}\left(\vec{\nabla}\left(\vec{\nabla}\cdot\vec{M}\right) - \vec{\nabla}\times\left(\vec{\nabla}\times\vec{M}\right)\right) \\ &= \frac{2A}{M_s^2}\left(\frac{M_s\pi^2}{\delta^2}\right)(\cos 2\theta\sin\theta\cos\varphi\,\hat{x} + \cos 2\theta\sin\theta\sin\varphi\,\hat{y} \\ &\quad - 2\sin^2\theta\cos\theta\,\hat{z}) \end{aligned} \quad \textbf{(19)}$$

where the wall width is given by $\delta = \pi\sqrt{\frac{A}{K}}$, assuming a Bloch wall. The torque due to this field

is:

$$\vec{M} \times \vec{H}_{ex} = 2K(-\sin\theta\cos\theta\sin\varphi\,\hat{x} + \sin\theta\cos\theta\cos\varphi\,\hat{y} - 0\hat{z}) \quad \textbf{(20)}$$

This exactly cancels the torque due to the anisotropy field. One might expect this is the case since the balance of exchange and anisotropy energy defines the wall profile, from which the wall width used in Equation (19) is derived.

A.1.1.5 Spin-Transfer Torques

The spin-transfer torque terms in (5) are those which depend on the magnetization gradient, $\frac{\partial \vec{M}}{\partial x}$ in this 1D approximation. The gradient can be decomposed into two derivatives, $\frac{\partial \vec{M}}{\partial x} = \frac{\partial \vec{M}}{\partial \theta}\frac{\partial \theta}{\partial x}$, where $\frac{\partial \vec{M}}{\partial \theta}$ can be computed by differentiating Equation (7) and $\frac{\partial \theta}{\partial x}$ from the domain wall shape:

$$\theta(x) = 2\tan^{-1}\left(e^{(x-\mathrm{x}_0)\pi/\delta}\right) \quad \textbf{(21)}$$

Equation (21) defines the polar angle θ of a magnetic moment in a domain wall centered about x_0. By evaluating the limits of Equation (21), we see the moments outside the wall are at $0\,rad$ on one side and $+\pi$ on the other (Figure A.1.2), with the transition defined by the given expression.

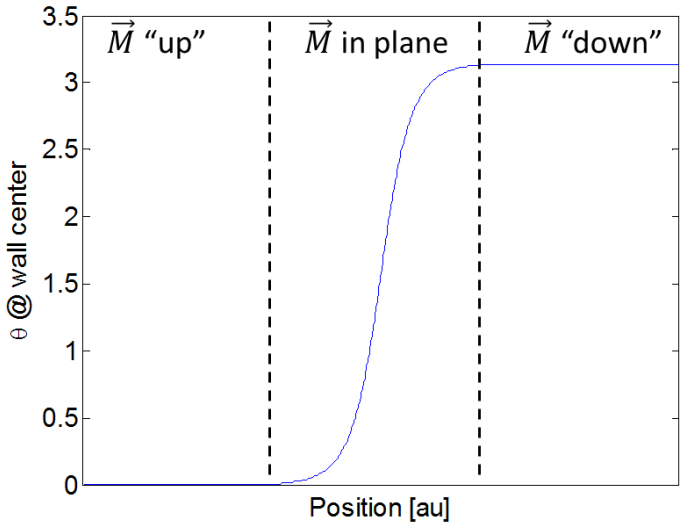

Figure A.1.2 – Domain wall center angle as a function of position; the magnetization lies in the plane of the film at the domain wall center.

To compute the gradient we differentiate with respect to x:

$$\frac{\partial\theta}{\partial x} = \frac{\pi}{\delta}\frac{2e^{(x-x_0)\pi/\delta}}{1+e^{2(x-x_0)\pi/\delta}} = \frac{\pi}{\delta}\sin\theta \tag{22}$$

Note that we exploited $\sin\theta = \sin\left[2\tan^{-1}\left(e^{(x-x_0)\pi/\delta}\right)\right] = \frac{2e^{\frac{(x-x_0)\pi}{\delta}}}{e^{2(x-x_0)\pi/\delta}+1}$.

The adiabatic spin-transfer torque is given by the third term of Equation (5). Using Equation (22) to compute the cross products and converting to spherical coordinates yields:

$$\vec{\tau}_{STT,ADB} = \begin{bmatrix}0\\-1\\0\end{bmatrix}\frac{u\pi}{\gamma\delta}M_s\sin\theta \tag{23}$$

The non-adiabatic spin-transfer torque is given by the fourth term of Equation (5). Using Equation (22) to compute the cross products and converting to spherical coordinates yields

$$\vec{\tau}_{STT,NONADB} = \begin{bmatrix}0\\0\\1\end{bmatrix}\frac{\beta u\pi}{\gamma\delta}M_s\sin\theta \tag{24}$$

A.1.1.6 Spin-Hall Effect Torque

For a current flow in the $\hat{x}$-direction, spins scattered from a non-magnetic underlayer up into the magnetic wire in which the domain wall resides will be polarized in the plane of the wire, orthogonal to the current direction. The exact orientation of the spins is determined by the materials used and the direction of the current, but we can express the magnitude of the spin-Hall effect as a field along the $\hat{y}$-axis regardless. For this exercise, let us assume the spin-Hall angle is negative and the electron flow is along the $+\hat{x}$-direction. The equivalent spin-Hall "field" is:

$$\vec{H}_{SHE} = \frac{\hbar J_{NM} |\theta_{SH}|}{2eM_s t_{FM}} (-\hat{y}) \tag{25}$$

The torque due to this field is given by the last term in Equation(5). Once again we take the relevant cross products and convert to spherical coordinates, yielding:

$$\vec{\tau}_{SHE} = \begin{bmatrix} 0 \\ -\cos\theta \sin\varphi \\ -\cos\varphi \end{bmatrix} M_s H_{SHE} \tag{26}$$

We will keep this term in the computation for the time being, but as we are ultimately trying to reach the STT equation in section it will be dropped later on. Note that for this torque to have any influence in driving the domain wall, the wall must have a Néel structure.

A.1.2 Computing the Domain Wall Velocity

The domain wall velocity is $\partial x/\partial t$, which can be thought of as the rate of change of position of the domain wall center. So far, we have found expressions that describe the time rate of change of the magnetization, or more specifically, the rate of change of the magnetization's polar and azimuthal angles at the domain wall center. We can combine all the torque terms we calculated to find the torque acting on the polar angle ($\vec{\tau}_\theta$) and that on the azimuthal angle ($\vec{\tau}_\varphi$):

$$\vec{\tau}_\theta = 4\pi M_s^2 \left(N_y - N_x\right) \sin\theta \sin\varphi \cos\varphi + M_s \left(H_x \sin\varphi - H_y \cos\varphi\right) \tag{27a}$$
$$+ \frac{\alpha M_s}{\gamma} \dot{\varphi} sin\theta + \frac{u\pi}{\gamma\delta} M_s \sin\theta - H_{SHE} M_s \cos\theta \sin\varphi$$

$$\vec{\tau}_{\varphi} = M_s H_x \cos\theta \cos\varphi + M_s H_y \cos\theta \sin\varphi - M_s H_z \sin\theta - \frac{\alpha M_s}{\gamma}\dot{\theta} \tag{27b}$$
$$+ \frac{\beta u \pi}{\gamma \delta} M_s \sin\theta - M_s H_s \cos\varphi$$
$$+ 4\pi M_s^2 \sin\theta \cos\theta \left(N_z - N_y \sin^2\varphi - N_x \cos^2\varphi\right)$$

We wish to find $\partial x/\partial t$, which we can do by computing $\frac{\partial x}{\partial t} = \frac{\partial \theta}{\partial t}\frac{\partial x}{\partial \theta}$ and understanding that $\frac{\partial \theta}{\partial t} = \dot{\theta} = -\frac{\gamma}{M_s}\vec{\tau}_{\theta}$ and $\frac{\partial \varphi}{\partial t} = \dot{\varphi} = -\frac{\gamma}{M_s}\vec{\tau}_{\varphi}$. At this point, we can also make simplifications; at the domain wall center, $\theta = \pi/2$ and so $\cos\theta = 0$ and $\sin\theta = 1$. This leaves:

$$\dot{\theta} = -4\gamma\pi M_s\left(N_y - N_x\right)\sin\varphi\cos\varphi - \gamma H_x \sin\varphi + \gamma H_y \cos\varphi - \alpha\dot{\varphi} + \frac{u\pi}{\delta} \tag{28a}$$

$$\dot{\varphi} = \gamma H_z + \alpha\dot{\theta} - \frac{\beta u \pi}{\delta} + \gamma H_{SHE}\cos\varphi \tag{28b}$$

Plugging the second of these equations into the first and simplifying yields:

$$\dot{\theta} = -\frac{\gamma}{1+\alpha^2}\Big[4\pi M_s\left(N_y - N_x\right)\sin\varphi\cos\varphi + H_x\sin\varphi + H_y\cos\varphi + \alpha H_z \tag{29}$$
$$- \frac{\alpha\beta u\pi}{\gamma\delta} + \alpha H_{SHE}\cos\varphi - \frac{u\pi}{\delta}\Big]$$

From here, we can solve for $\frac{\partial x}{\partial t}$:

$$v_{DW} = \frac{\partial x}{\partial t} = \frac{\partial \theta}{\partial t}\frac{\partial x}{\partial \theta} \tag{30}$$
$$= -\frac{\gamma\delta}{\pi(1+\alpha^2)}\Big[4\pi M_s\left(N_y - N_x\right)\sin\varphi\cos\varphi + H_x\sin\varphi$$
$$+ H_y\cos\varphi + \alpha H_z - \frac{\alpha\beta u\pi}{\gamma\delta} + \alpha H_{SHE}\cos\varphi - \frac{u\pi}{\delta}\Big]$$

This is the general expression for the domain wall velocity in the 1D model. However, we can make further simplifying calculations and assumptions to produce the form given in section

5.1:

$$v_{DW} = \left(\frac{1+\alpha\beta}{1+\alpha^2}\right)\frac{g\mu_B PJ}{2eM_S} = \left(\frac{1+\alpha\beta}{1+\alpha^2}\right)u \quad \textbf{(31)}$$

First, we can set all applied field terms to 0, in addition to the SHE term, which was not included in that analysis. Finally, we recognize that when a domain wall moves under large current densities (above Walker breakdown), its internal moments are actually precessing. If we average Equation (30) over a precessional period, the demagnetizing field term drops out:

$$\langle \sin\varphi \cos\varphi \rangle = \frac{1}{2}\langle \sin 2\varphi \rangle = \frac{1}{2}\left(\frac{1}{2\pi}\int_0^{2\pi} \sin 2\varphi \, d\varphi\right) = 0 \quad \textbf{(32)}$$

This leaves the expression in Equation (31).